Electronic Supplementary Material (ESI) for Inorganic Chemistry Frontiers.

Regulation of bulk reconstruction of $FeNiMoO_4$ via NH_3 treatment for high performance water oxidation

Fanan Wang,[a,b] Lianggao Hu,[a] Renzhi Deng,[a] Dongfei Lu,[a] Xin Chen,[c] Xinyi Ren,[d] Dibo dong,[b] Rengui Weng,*[a] Gang Xu *[c] and Hongbin Yang [d]

[a] *Fujian Eco-materials Engineering Research Center, School of Ecological Environment and Urban Construction, Fujian University of Technology, No3 Xueyuan Road, Fuzhou 350118, China*

[b] *Institute of Smart Marine and Engineering, Fujian University of Technology, No3 Xueyuan Road, Fuzhou 350118, China*

[c] *Fujian Provincial Key Laboratory of Advanced Materials Oriented Chemical Engineering, College of Chemistry and Material Science, Fujian Normal University, No.8 Shangsan Road, Fuzhou 350007, China*

[d] *Dalian Institute of Chemical Physics, Chinese Academy of Sciences, 457 Zhongshan Road, Dalian 116023, China*

*Corresponding author.

E-mail address: wengrengui109@fjut.edu.cn (R.G. Weng); xugang@fjnu.edu.cn (G. Xu)

Table S1. The ICP-OES results of Fe and Mo content in the powder ultrasonicated off the related electrodes, each of which was repeatedly tested by 3 times.

	FeMoNi-O-fresh	FeMoNi-O-2h	FeMoNi-O-24h	FeMoNi-N-fresh	FeMoNi-N-2h	FeMoNi-N-24h
Fe	2.1 ± 0.07 %	4.0 ± 0.08 %	4.3 ± 0.09 %	1.9 ± 0.10 %	6.1 ± 0.05 %	6.2 ± 0.08 %
Mo	49.7 ± 1.4 %	--*	--*	51.0 ± 1.1 %	--*	--*

*: undetectable

Table S2. The BET surface area of the samples before and after the reconstruction.

	FeMoNi-O-fresh	FeMoNi-O-2h	FeMoNi-N-fresh	FeMoNi-N-2h
BET Surface area ($cm^2 \cdot g^{-1}$)	61.1	28.6	34.7	172.2
Pore volume ($cc \cdot g^{-1}$)	0.12	0.08	0.06	0.24

Table S3. The portion of the deconvoluted species in Ni, Mo and O, and Mo, Ni and Fe in the total metal elements, respectively, from the XPS analyses of the powder ultrasonicated off the related fresh electrode.

	FeMoNi-O-fresh	**FeMoNi-N-fresh**
Ni^{1+}	0	8.7%
Ni^{2+}	62.2%	65.5%
Ni^{3+}	37.8%	25.8%
Mo^{6+}	92.6%	57.2%
Mo^{5+}	7.4%	17.3%
Mo^{4+}	0	25.5%
M-O	80.2%	67.5%
O_{vac}	6.5%	23.8%
H_2O	13.3%	8.7%
Mo	75.1%	69.2%
Ni	23.2%	28.7%
Fe	1.7%	2.1%

Table S4. The portion of the deconvoluted species in Ni and Fe, and Mo, Ni and Fe in the total metal elements, respectively, from the XPS analyses of the powder ultrasonicated off the related electrode.

	FeMoNi-O-10min	FeMoNi-O-2h	FeMoNi-N-10min	FeMoNi-N-2h
Ni^{2+}	70.4%	74.3%	59.3%	57.6%
Ni^{3+}	29.6%	25.7%	40.7%	43.4%
Fe^{3+}(A)	-	66.3%	-	31.2%
Fe^{3+}(B)	-	33.7%	-	68.8%
Ni	71.2%	96.3%	84.4%	94.1%
Fe	3.5%	3.7%	4.0%	5.9%
Mo	25.3%	undetectable	11.6%	undetectable

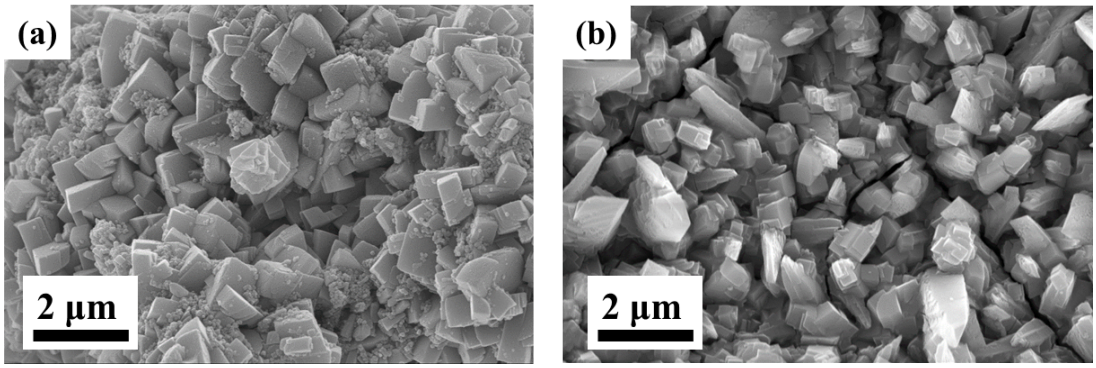

Fig. S1. SEM images of (a) FeMoNi-N/NF and (b) FeMoNi-O/NF.

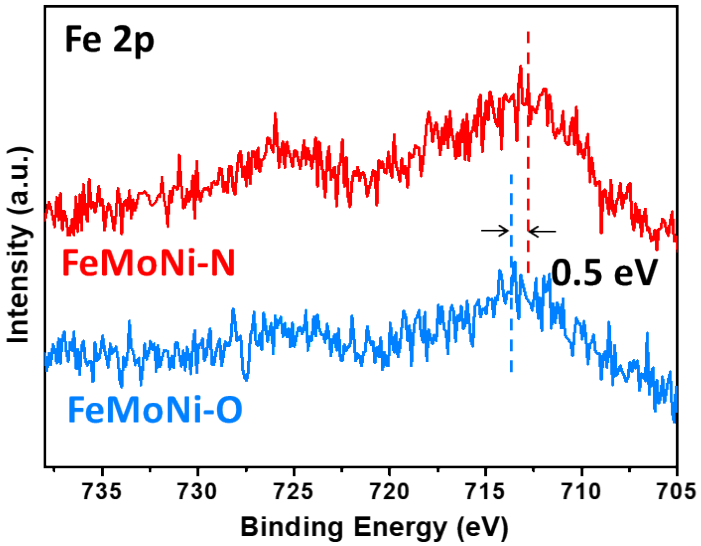

Fig. S2 XPS spectra of Fe 2p on FeMoNi-N and FeMoNi-O.

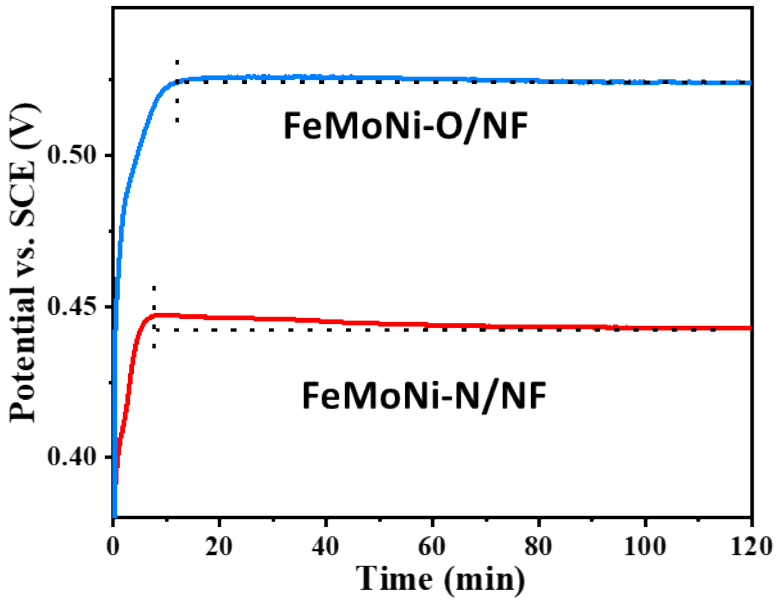

Fig. S3. Chronopotentiometry curves (V-T) for FeMoNi-O/NF and FeMoNi-N/NF under galvanostatic oxidation at 50 mA·cm^{-2} in 1 M KOH solution.

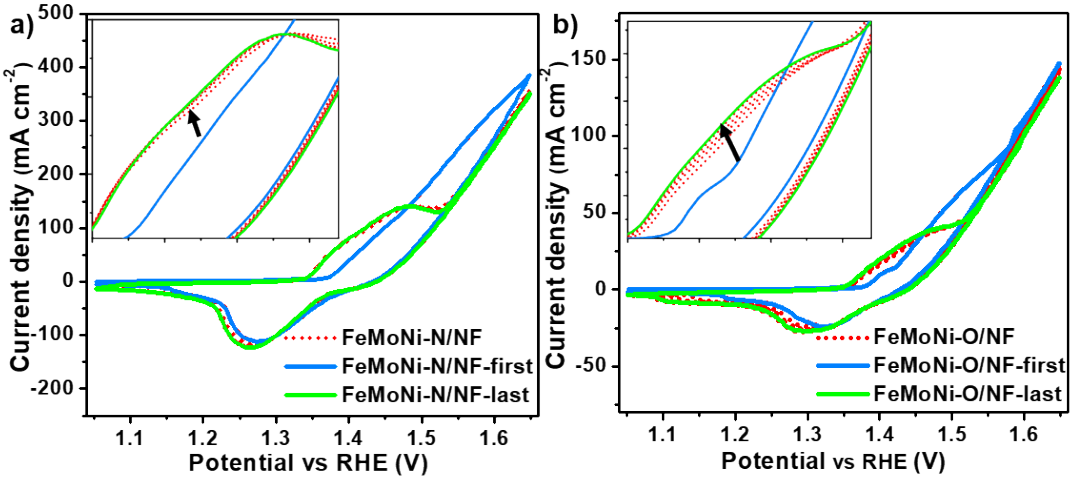

Fig. S4. CV activation curves for (**a)** FeMoNi-N/NF and (**b)** FeMoNi-O/NF, inset with the enlargement from 1.35-1.52 V vs. RHE.

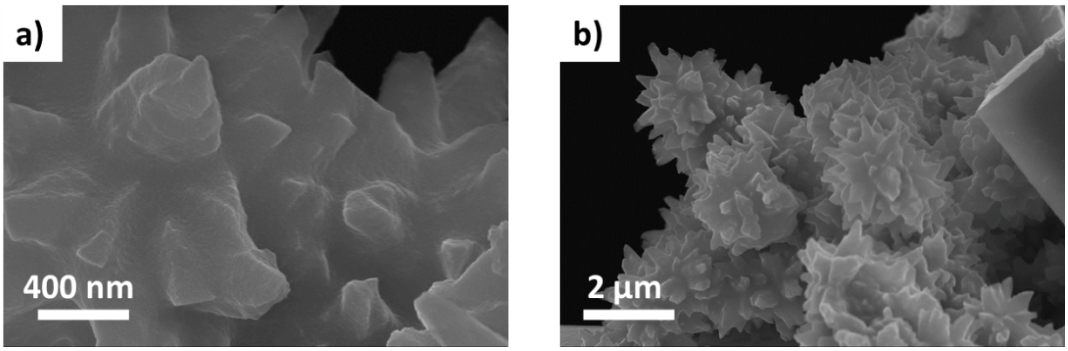

Fig. S5. SEM images of FeMoNi-O/NF-10min at different magification.

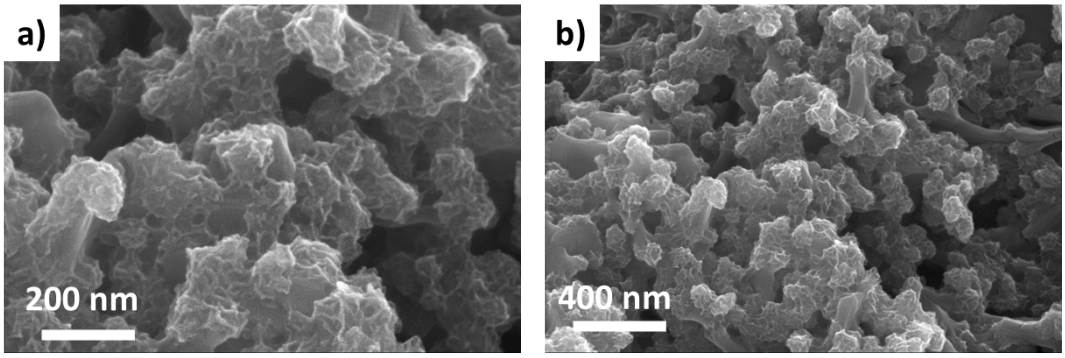

Fig. S6. SEM images of FeMoNi-N/NF-10min at different magification.

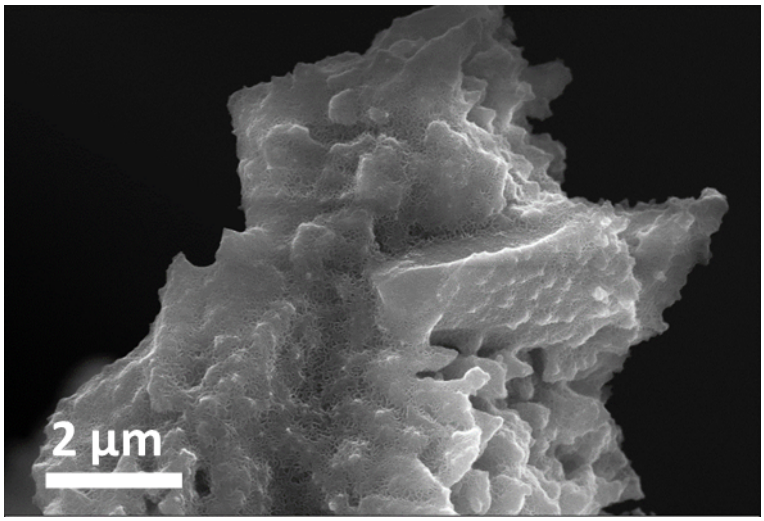

Fig. S7. SEM images of FeMoNi-N/NF-2h.

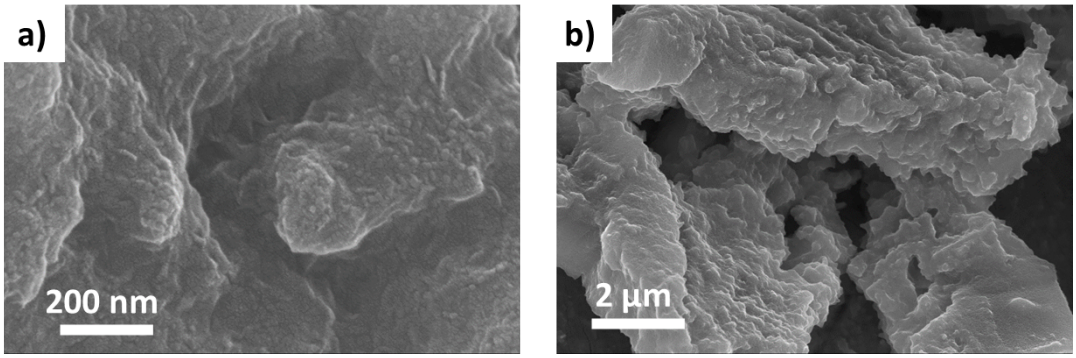

Fig. S8. SEM images of FeMoNi-O/NF-2h at different magification.

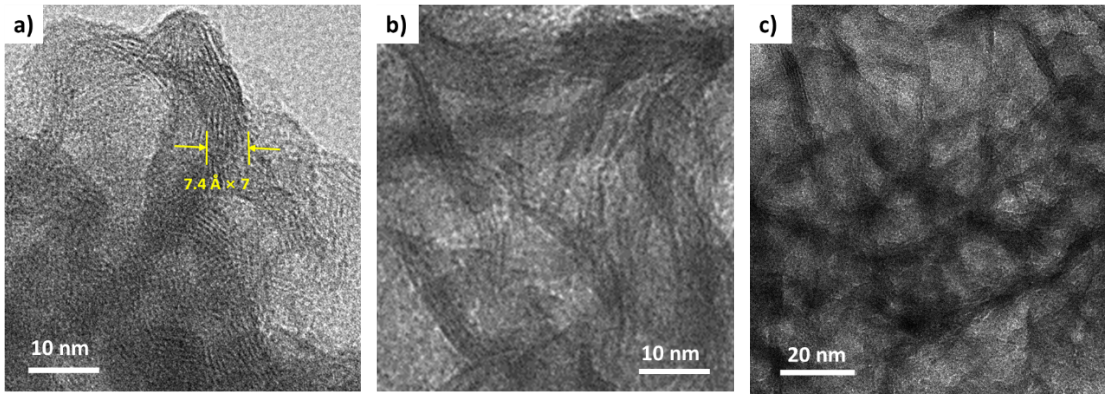

Fig. S9. HRTEM images of FeMoNi-N/NF-2h at different magification.

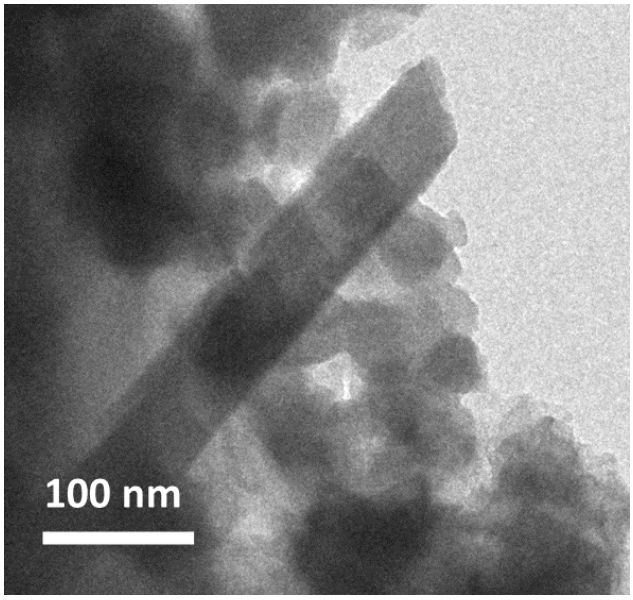

Fig. S10. HRTEM images of FeMoNi-O/NF-10min.

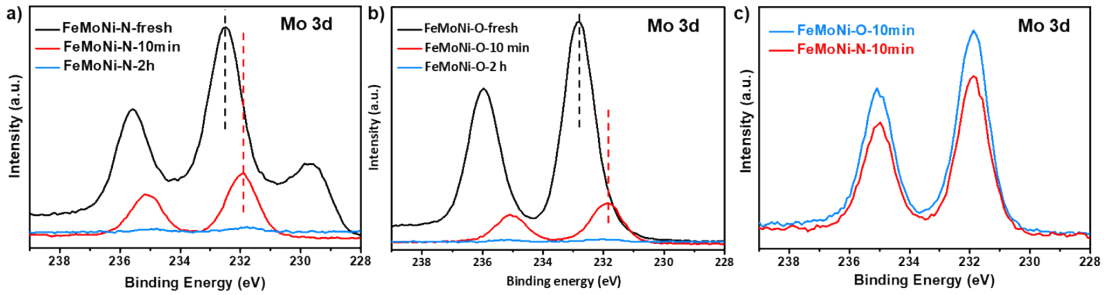

Fig. S11. XPS spectra of Mo 3d on FeMoNi-N/NF and FeMoNi-O/NF after different periods of reaction.

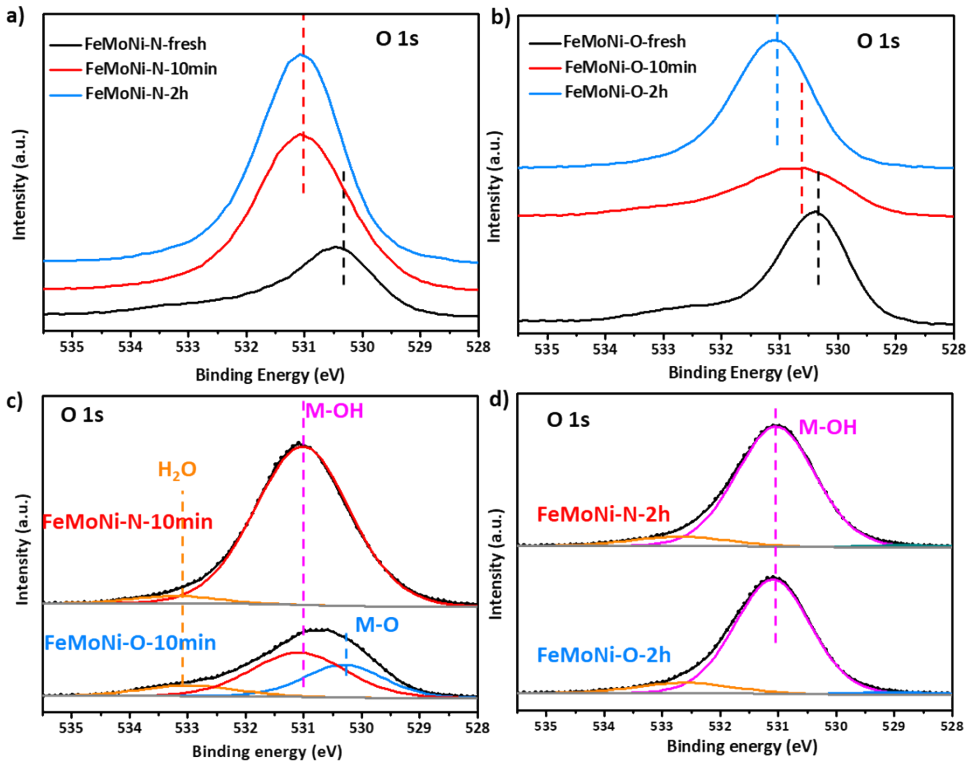

Fig. S12. XPS spectra of O 1s on FeMoNi-N/NF and FeMoNi-O/NF after different periods of reaction.

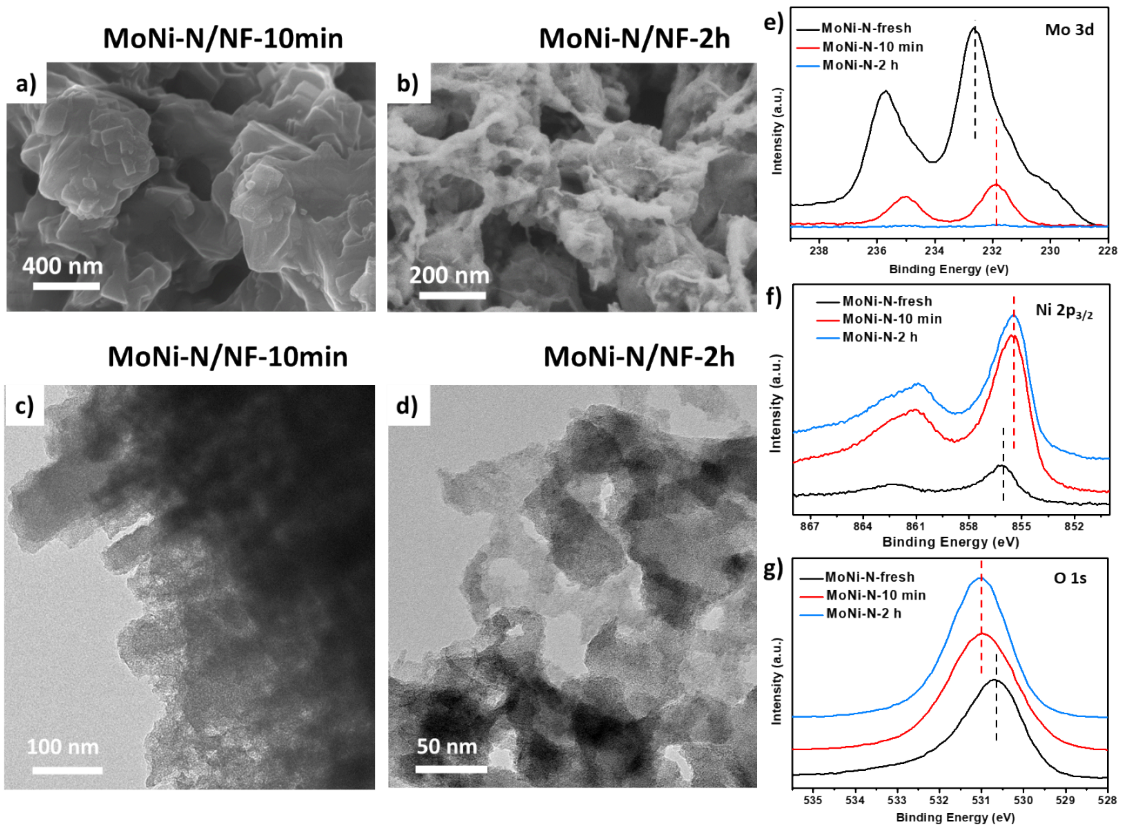

Fig. S13. SEM images of (a) MoNi-N/NF-10min and (b) MoNi-N/NF-2h; the HRTEM images of (c) MoNi-N/NF-10min and (d) MoNi-N/NF-2h; XPS spectra of (e) Mo 3d, (f) Ni $2p_{3/2}$ and (g) O 1s on MoNi-N/NF after different periods of reaction.

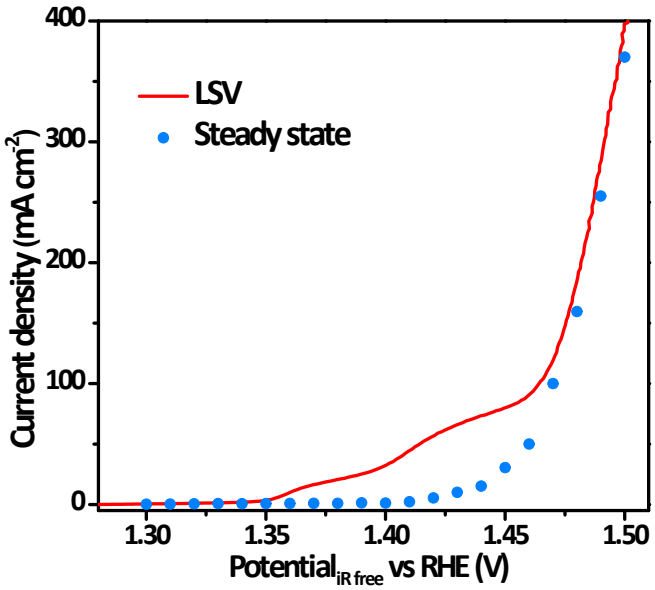

Fig. S14. Steady state test by potential on FeMoNi-N/NF, with comparison to the LSV curve. As can be seen, the $Ni(OH)_2$-to-NiOOH oxidation current in the range of 1.35-1.45 V vs. RHE rarely exists, and the oxidation current could be mostly contributed to the OER.

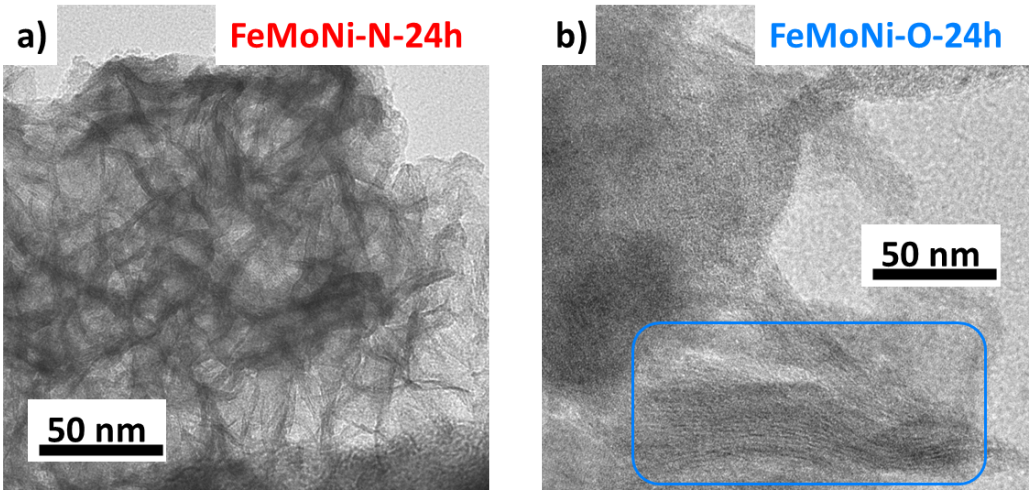

Fig. S15. The HRTEM images of a) FeMoNi-N/NF-24h, b) FeMoNi-O/NF-24h. As shown, the lamellar structures of the FeMoNi-N maintain distinct after 24h; while the FeMoNi-O appears amorphous structure mostly, with partly evolved to thick lamellar structures.

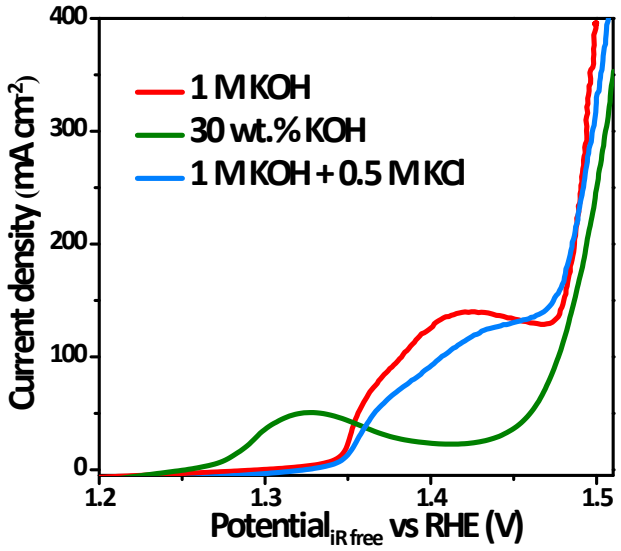

Fig. S16. LSVs taken in industrial grade alkaline (30 wt.% KOH solution) and simulated seawater (1 M KOH + 0.5 M KCl solution) on FeMoNi-N/NF.

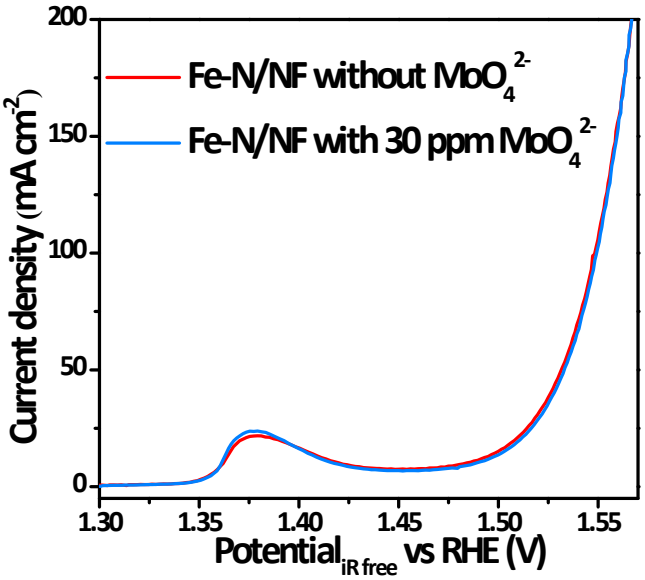

Fig. S17. LSVs taken on Fe-N/NF in electrolytes with or without MoO_4^{2-}.

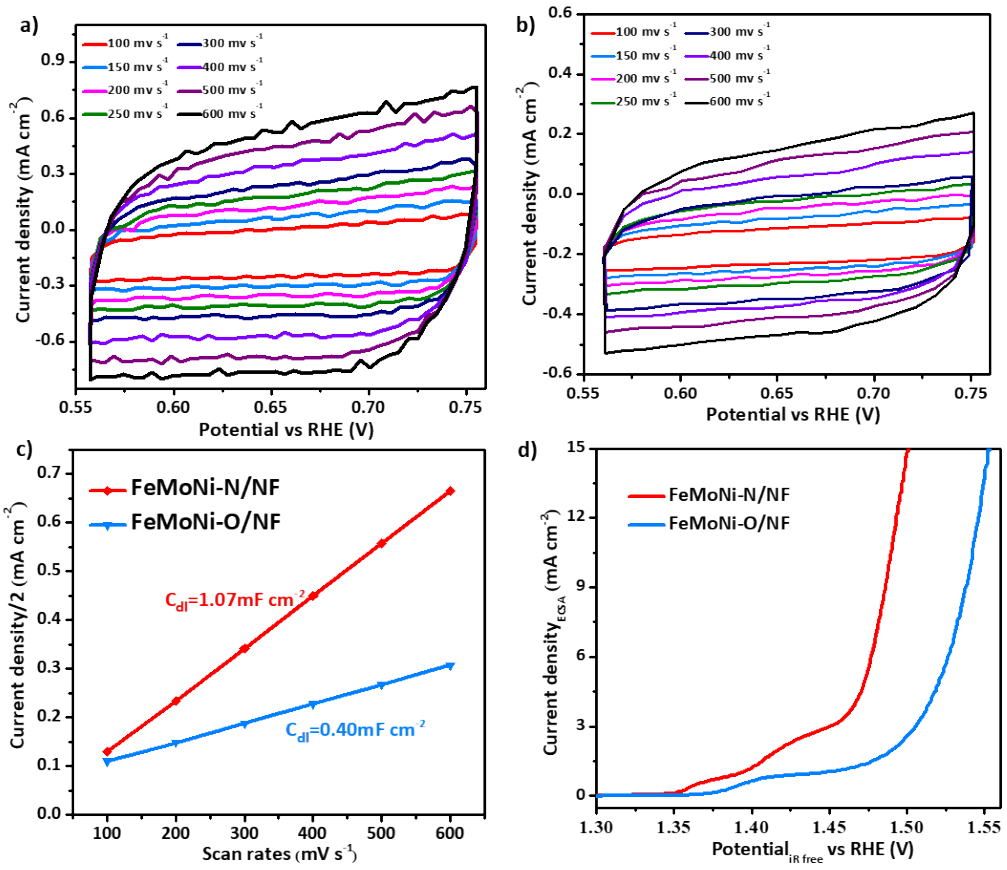

Fig. S18. CV curves on (a) FeMoNi-N/NF and (b) FeMoNi-O/NF; the comparision of (c) C_{dl} and (d) ECSA nomolized LSV for FeMoNi-N/NF and FeMoNi-O/NF.

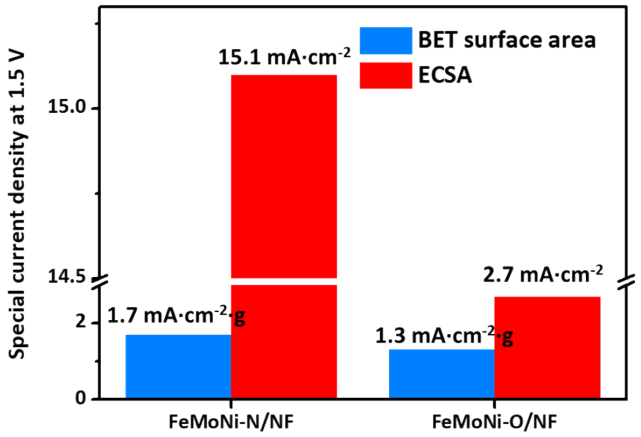

Fig. S19. The special activity based on BET surface area and ECSA for FeMoNi-N/NF and FeMoNi-O/NF.

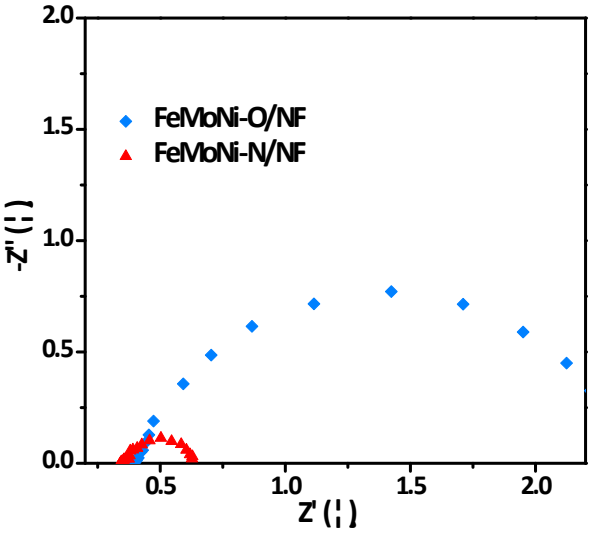

Fig. S20. The Nyquist plots acquired by EIS for FeMoNi-N/NF and FeMoNi-O/NF.

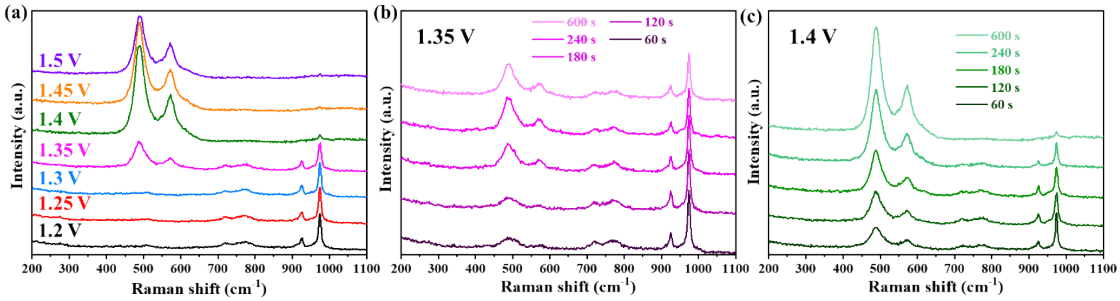

Fig. 21. The *in-situ* Raman spectra collected at different potentials with varied reaction time on FeMoNi-O/NF.